UDC 669.15-194.55:621.785.7

TEMPERING-INDUCED STRUCTURAL CHANGES IN STEEL 10Kh9K3V1M1FBR AND THEIR EFFECT ON THE MECHANICAL PROPERTIES

A. Yu. Kipelova,[1] A. N. Belyakov,[1] V. N. Skorobogatykh,[2] I. A. Shchenkova,[2] and R. O. Kaibyshev[1]

Processes of segregation of carbides and evolution of dislocation structure in tempering of steel 10Kh9K3V1M1FBR in the temperature range of 300 – 800°C and their effect on the mechanical properties are studied.

Keywords: steels of martensitic class, tempering, carbide transformations, dislocation structure, mechanical properties, microstructure, off-orientation maps.

INTRODUCTION

Creation of new-generation high-chromium steels of martensitic class of type P91/P92/P911 in the USA, Japan, and countries of the European Community [1] has made it possible to begin large-scale erection of coal-fired power plants with steam temperature of 580 – 650°C and pressure of up to 340 MPa. The mode of heat treatment of these steels consists of normalizing and medium-temperature tempering. The troostomartensitic structure formed in the heat treatment ensures high creep resistance of such steels [1]. The stability of this structure in service is determined by the volume fraction and distribution of particles of types Me(C, N) and $Me_{23}C_6$ segregated during tempering. These carbides play the key role in the creep strength. The nature, size, and distribution of the carbides determine the stability of the dislocation structure of the troostomartensite and thus the operating temperature of the steels [1]. The choice of the optimum content of the carbide-forming elements (0.2% V + 0.07% Nb) for formation of coagulation-resistant Me(C, N) carbonitrides in tempering has ensured suppression of cell formation in aging and creep and made it possible to use steels of the new generation with 9% Cr at operating temperatures 70 – 120°C higher than that of similar martensitic steels of the previous generation [1 – 5].

In contrast to the evolution of martensitic structure in steels with 9 – 11% Cr of the preceding generations the carbide reactions in tempering have been studied in quite detail [6 – 15]. It has been shown that two main reactions occur in parallel in the process of tempering. The first reaction yields a $Me_{23}C_6$ carbide and the second yields a Me(C, N) carbonitride. The first reaction proceeds in several stages [6 – 13]. The $Me_{23}C_6$ carbide is a stable phase; in tempering its appearance is preceded by formation of Me_3C, Me_2C, Me_7C, and Me_7C_3 carbides metastable with respect to it. We know of two types of stages of carbide transformations leading to formation of $Me_{23}C_6$. In steels with 0.7 – 1.5% nickel [13, 16] the carbide transformation proceeds in the following stages:

$$Me_3C \rightarrow Me_2C \rightarrow Me_{23}C_6. \quad (1)$$

It should be noted that the presence of nickel in the α-matrix stabilizes the Me_2C carbide. Reaction (1) does not proceed to the end if the temperature of the final tempering ≤ 690°C [13, 16]. Me_2C and $Me_{23}C_6$ carbides are observed in the structure of the steels of the previous generation simultaneously even after 10^5 h creep at ≤ 500°C [16].

In all probability the mechanism of change of all the stages of reaction (1) is independent nucleation of a more stable phase. For the reaction $Me_3C \rightarrow Me_2C$ this is connected with the difference in the chemical compositions of the carbides. In alloyed cementite the fraction of Fe is no lower than 75% of the metallic atoms [10, 17]. In the $Me_2(C, N)$ carbonitride chromium comprises more than half

[1] Belgorod State University, Belgorod, Russia (E-mail: rustam kaibyshev@bsu.edu.ru).

[2] Central Research Institute for Machine Building Technology (GNTs RF OAO NPO "TsNIITMASh"), Moscow, Russia.

of the metallic atoms, and the content of molybdenum may reach up to 30% (mass) [12]. When the main nonmetallic atom of the $Me_2(C, N)$ carbonitride is nitrogen, the chromium content in it comprises 95 at.% [15]. In the case of the second stage only separate location of the $Me_2(C, N)$ and $Me_{23}C_6$ phases has been observed experimentally [16]; the particles of the $Me_2(C, N)$ carbonitride have the shape of plates with a length of over 100 nm and those of the $Me_{23}C_6$ carbide have a round shape.

Another series of carbide transformations in steels bearing ≤ 0.6% Ni [8, 10] is as follows:

$$Me_3C \rightarrow Me_7C_3 \rightarrow Me_{23}C_6. \quad (2)$$

The Me_7C_3 carbides dissolve completely after tempering at 650°C for 100 h. The most probable mechanism of change in the stages of the $Me_3C \rightarrow Me_7C_3$ transformation is independent nucleation [11], because the chemical compositions of these two carbides differ considerably in the contents of chromium and iron, as in the first stage of reaction (1). At the same time, the authors of [11] assume that this transformation can occur only by the mechanism of internal rearrangement of the lattice of cementite initiated by diffusion of chromium from martensite. Opinions differ about the mechanism of the second stage of $Me_7C_3 \rightarrow Me_{23}C_6$, i.e., this transformation may occur both by the mechanism of rearrangement of the Me_7C_3 lattice into the lattice of $Me_{23}C_6$, which is more probable [11], and by the mechanism of independent nucleation of the $Me_{23}C_6$ carbide. It should be noted that both Me_7C_3 and $Me_{23}C_6$ are arranged in the martensite matrix according to exact orientation relations [8, 11]. This means that they nucleate as particles with coherent boundaries. The Me_7C_3 carbide contains ≥ 80 at.% Cr [10]. Its chemical composition is close to that of $Me_{23}C_6$; these two carbides differ in their lattices. In fact, the less stable Me_7C_3 carbides dissolve during the formation of $Me_{23}C_6$ carbides. If the tempering temperature is lower than 700°C and the segregation of $Me_{23}C_6$ [14] over dislocation boundaries of martensite laths does not lead to their complete dissolution, the last stage of reaction (2) even in the case of creep at 500°C proceeds to the end in a relatively short time [8].

As a rule, the Nb(C, N) carbonitride is present in the metal after hardening [13]. The size and volume fraction of these carbonitrides is determined by the content of niobium in the steel. In martensitic steels of the preceding generation, which bear about 0.2% Nb [17], the Me(C, N) carbonitride does not dissolve in heating for hardening even until 1200°C; after hardening, the structure contains coarse Me(C, N) carbonitrides enriched with niobium. Tempering is accompanied by additional segregation of secondary dispersed Me(C, N) carbonitrides [13]. At $t_{temp} \leq 650$°C niobium-enriched carbonitrides are segregated; vanadium-enriched Me(C, N) carbonitrides are segregated at higher temperatures. It should be noted that after tempering at 690°C the dominant part of vanadium (> 0.15%) in steels of the previous generation [13] is retained in the solid solution. In these steels the stable carbonitride is single Me(C, N); separation into niobium- and vanadium-enriched carbonitrides, as in modern steels with 0.07% Nb – 0.2% V [7, 18] where a mixture of these carbonitrides is the stable component, does not occur. In creep, in aging, and even in tempering, the secondary nanosize carbonitrides of type Me(C, N) dissolve and the primary Me(C, N) carbonitrides with a size ≥ 0.2 μm, which are commonly [8] located over large-angle boundaries (LAB), coarsen. Thus, these carbonitrides do not make a noticeable contribution either to the precipitation hardening or to the stabilization of the dislocation structure of the troostomartensite. From the standpoint of the design of the microstructure this is the main difference between the high-chromium steels of the previous generation and modern steels.

In modern steels of type P91 carbide reactions in tempering in a temperature range of 750 – 780°C yield stable carbides with a size ≤ 100 nm. It has been shown in [9] that in the early version of steel P91 the succession of carbide segregation at $t_{temp} \geq 550$°C is as follows

$$Me_3C \rightarrow \begin{cases} Me_2(C, N) + V(C, N) \\ Me_2(C, N) \\ V(C, N) \end{cases} \rightarrow Me_{23}C_6. \quad (3)$$

Alloyed cementite segregates due to self-tempering in the process of normalization; data on its segregation due to tempering are absent [9]. It should be noted that a part of reaction (3) in the form reaction (1) is observed for steel P9 [9]. In contrast to the latter, in steel P91 the $Me_2(C, N)$ carbonitride formed at 550 – 650°C is replaced by carbide $Me_{23}C_6$ and carbonitride V(C, N) at $t_{temp} \geq 700$°C [9]; no feature of reaction (2) has been detected. Note that in contrast to the steels of the previous generation, the particles of the $Me_2(C, N)$ carbonitride in steels of type P91 have a round shape and their size of about 40 nm is comparable to the size of the Me(C, N) carbonitrides [32]. They are metastable and transform into Me(C, N) vanadium-enriched carbonitrides in the process of tempering at 750°C and higher temperatures or in creep at 600°C [32].

In steel P91 an equilibrium mixture of Me(C, N) carbonitrides enriched with vanadium (round particles with a size of 10 nm and plates with a thickness of less than 50 nm) and niobium (round particles with a size of 25 – 50 nm) has been observed [9, 18]. Mixed carbonitrides have not been detected. The two-phase decomposition of Me(C, N) carbonitrides is assumed [7] to be the main cause of the high creep resistance of these steels [4, 19, 20], because the thermodynamic equilibrium prevents coagulation of niobium-enriched Me(C, N)-type carbonitrides due to the dissolution of the vanadium-enriched carbonitrides. These carbonitrides are arranged in the α-matrix according to the orientation relation of Baker – Nutting [21], i.e., $(100)_{Me(C, N)} \parallel (100)_\alpha$, $[010]_{Me(C, N)} \parallel [011]_\alpha$, which reflects the coherent nature of

their phase boundaries [21]. It has been shown in [19, 21] that the vanadium-enriched Me(C, N) carbonitrides have the form of "wings" (plates) even if these wings are not isolated but adjoin round particles of the niobium-enriched carbonitride. The formation of these wings causes dissolution of $Me_2(C, N)$ needles about 26 nm in diameter [19]. Growth in the content of niobium to 0.086% and in the content of nitrogen to 0.06%, which exceeds somewhat the upper limit of their content in steel P91 [22], causes full replacement of $Me_2(C, N)$ by a niobium-enriched Me(C, N) carbide in tempering [19]. It has not been determined yet whether the regular features of the carbide reactions for steel P91 that accompany tempering are typical for steel P911 and P92. We have every reason to assume that the $Me_2(C, N)$ carbonitride in steel P911 is a stable phase. If this is so, this is connected with the effect of the content of $\Sigma(W + Mo)$ on the carbide reactions in steels of martensitic class of the new generation.

The aim of the present work consisted in studying the carbonitride reactions and the evolution of the dislocation structure, which occur in tempering of steels of martensitic class of the new generation with 9% Cr, using steel 10Kh9K3V1M1FBR as an example, and to determine the dependence of its mechanical properties on the tempering temperature.

METHODS OF STUDY

We studied high-temperature steel 10Kh9K3V1M1FBR with the following chemical composition (in wt.%): 0.13 C, 8.6 Cr, 3.2 Co, 1.2 W, 0.9 Mo, 0.2 V, 0.1 Cu, 0.07 Nb, 0.04 N, 0.005 B, 0.02 Mn, 0.05 Ni, 0.06 Si, the remainder Fe. The test heats were obtained at the experimental grounds of "TsNIITMASh." The specimens were hardened in air from 1050°C and tempered in the temperature range of 300 – 800°C for 3 h. We determined the effect of the temperature on the characteristics of static strength and ductility. For this purpose a specimen tempered at the specified temperature in a conventional furnace was cooled and then heated again to the same temperature in the furnace of an "Instron 5882" universal testing machine and tested for tensile strength at deformation rate of 2.1×10^{-3} sec^{-1}. We used flat specimens with functional part with a length of 12 mm and a cross section of 3×1.5 mm.

We determined the effect of the tempering temperature on the hardness and impact toughness at room temperature. The Brinell hardness was measured with the help of a Wolpert 3000BLD digital hardness meter at a load of 29,400 N using a ball from a hard alloy 10 mm in diameter. The *KCV* impact toughness was determined for standard specimens using an "Instron IMP460" pendulum impact machine with recording of the diagram.

The x-ray diffraction analysis of the metal was performed with the help of a "Rigaku Ultima 4" diffractometer with semiconductor detector in copper K_α radiation. Diffractograms of a standard (ferritic steel) and of the high-temperature steel were obtained by separating the doublet of the K_α spectrum line by the method of Rechinger. We measured the integral width of the line from plane (110) of the standard and of the studied steel using reflections of orders 1 and 2. The values of the microdeformations (MD) and the sizes of regions of coherent scattering (RCS) were determined by the method of Williamson – Hall.

Fracture surfaces and characteristics of the structure of martensite were studied using an FEI "Qanta 600F" scanning electron microscope equipped with an analyzer of diffraction of back-scattered electrons (EBSD). The data of the EBSD analysis were used for plotting the maps of off-orientations with allowance for the angular off-orientations exceeding 2°. The chemical and phase compositions of the secondary phases and the fine structure were analyzed using a transmission Jeol "JEM-2100" electron microscope (TEM) with accelerating voltage of 200 kV equipped with an Oxford Instruments attachment for energy dispersive analysis.

Local chemical analysis was performed only for heavy elements, i.e., metallic atoms. For this reason, in the present paper we give the fraction of atoms of any element in proportion to the atomic fraction of all the metallic atoms.

For the electron microscope analysis we prepared foils by the method of jet electrochemical polishing using a 10% solution of perchloric acid in acetic acid as an electrolyte in a Struers "TenuPol-5" device. The transverse size of the martensite laths was computed by the method of secants. The dislocation density inside the martensite laths was determined from the number of points of outcome of individual dislocations on the surface of a foil by the method of [23]. The volume fraction of a phase was evaluated in terms of the proportion of its area on a cross section of a specimen by the standard metallographic technique. The chemical composition and the nature of the particles of second phases were analyzed by the method of carbon replicas. In order to check the chemical composition of the $Me_{23}C_6$ carbides the replicas were studied under an FEI "Quanta 600F" scanning electron microscope equipped with a wave analyzer in addition to the attachment for energy dispersive analysis. The difference in the chemical composition of the carbides determined with the use of the two microscopes did not exceed the error of measurement.

Differential scanning calorimetry (DSC) was performed during heating and cooling of disc specimens with a mass of 30 – 50 mg at a rate of 2, 10, and 20 K/sec in an SDT Q600 device (TA Instruments). The initial and final temperatures of martensitic transformations were determined for specimens with a length of 25 mm and a diameter of 6 mm using a Netzsch DIL 402C dilatometer. The error of the measurements did not exceed 8%.

RESULTS

Temperatures of Phase Transformations. The DSC curves obtained for steel 10Kh9K3V1M1FBR are presented

TABLE 1. Temperatures of Phase Transformations in Steel 10Kh9K3V1M1FBR

v, K/min	Ac_1	A_2	Ac_3	M_i	M_f
2	830	778	861	390	318
10	845	778	862	383	302
20	841	777	890	369	290

in Fig. 1; the critical temperatures are presented in Table 1. In cooling, the DSC curves exhibit inflections corresponding to the beginning and end of martensitic transformation, i.e., the martensitic transformation in the studied steel develops completely for all the cooling rates used in the work. It should be noted that the use of dilatometric analysis ensures quite accurate determination of points M_i and M_f [24]. For this reason we present in Table 1 the values of these temperatures amended in accordance with the results of the dilatometric study.

The DSC curve obtained in heating at a rate $v_h = 2$ K/min exhibits an exothermic peak, which is usually associated with formation of $Me_{23}C_6$ carbide [25]. This phase starts to be segregated at $t_i = 535$°C and ends at $t_f = 640$°C. Elevation of the heating rate shifts both the exothermic and the endothermic peaks toward higher temperatures. At any rate of heating we detected endothermic peaks at about 778°C connected with transition of the steel from ferromagnetic state into a paramagnetic one. The endothermic peaks at higher temperatures correspond to the critical points of steel 10Kh9K3V1M1FBR (Table 1).

Microstructure after hardening and tempering. The fine structure of martensite in steel 10Kh9K3V1M1FBR is presented in Fig. 2*a*; the map of off-orientations of hardened martensite is presented in Fig. 3*a*. The parameters of the structure are given in Table 2. It can be seen that normalization causes formation of martensite, i.e., from the standpoint of the heat treatment theory the operation of normalizing for steel 10Kh9K3V1M1FBR is hardening with polymorphic transformation. None of the methods of study used in the work has shown features of presence of retained austenite. The electron microscope study showed the presence of round-shape carbonitrides of type Me(C, N) about 31 nm in size inside the martensite matrix. In most carbonitrides the fraction of niobium reached 80 – 89%, that of chromium was 3 – 7%, and that of vanadium was 7 – 10%. After normalization we observed rare plates of a Me_3C-type carbide segregated due to self-tempering.

The mean size of the initial austenite grains (IAG) was 14 μm. The packets of martensite laths were arranged randomly (Fig. 3*a*). The boundaries of the packets were primarily LAB. Small-angle boundaries (SAB) of packets were encountered rarely. Inside the martensite packets we discerned individual blocks separated by SAB. The off-orientation of these boundaries was low (below 5° in most cases). As a result, the volume fraction of the SAB amounted to 73%. Martensite laths and blocks considerably differing in the orientation and surrounded by LAB were observed sometimes inside individual martensite packets. The transverse size of the laths of packet martensite after hardening was about 200 nm (Table 2). The dislocation density exceeded 10^{15} m^{-2}; at such a density it is hard to resolve individual dislocations. The great number of lattice dislocations located inside martensite laths was responsible for high long-acting elastic stresses (Fig. 2*a*). The x-ray diffraction analysis confirmed

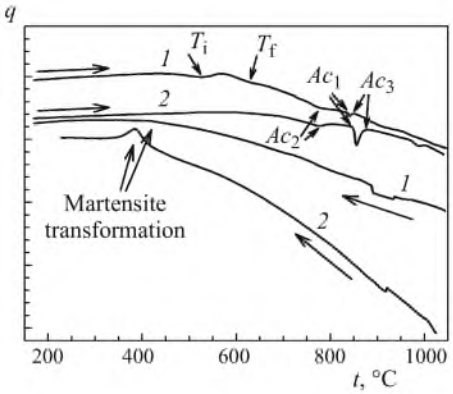

Fig. 1. DSC curves for steel 10Kh9K3V1M1FBR after heating and cooling at different rates (q is the heat flux): *1*) $v = 2$ K/min; *2*) $v = 20$ K/min.

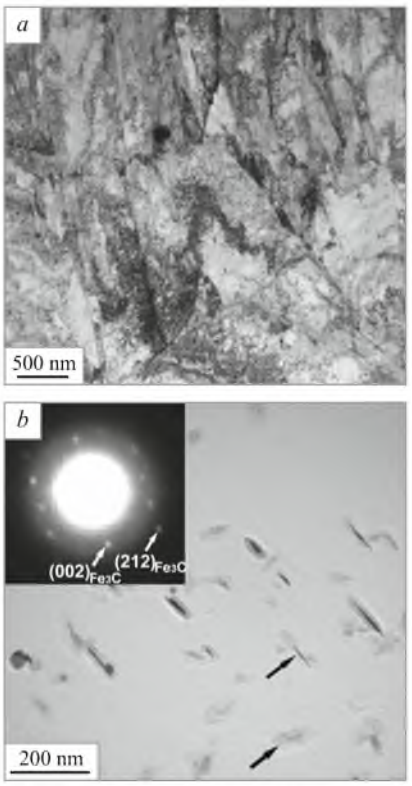

Fig. 2. Microstructure of steel 10Kh3V1M1FBR after hardening from 1050°C (*a*), cementite particles (indicated by the arrows) against a carbon replica, and microdiffraction from them after hardening and tempering at 300°C for 3 h (*b*).

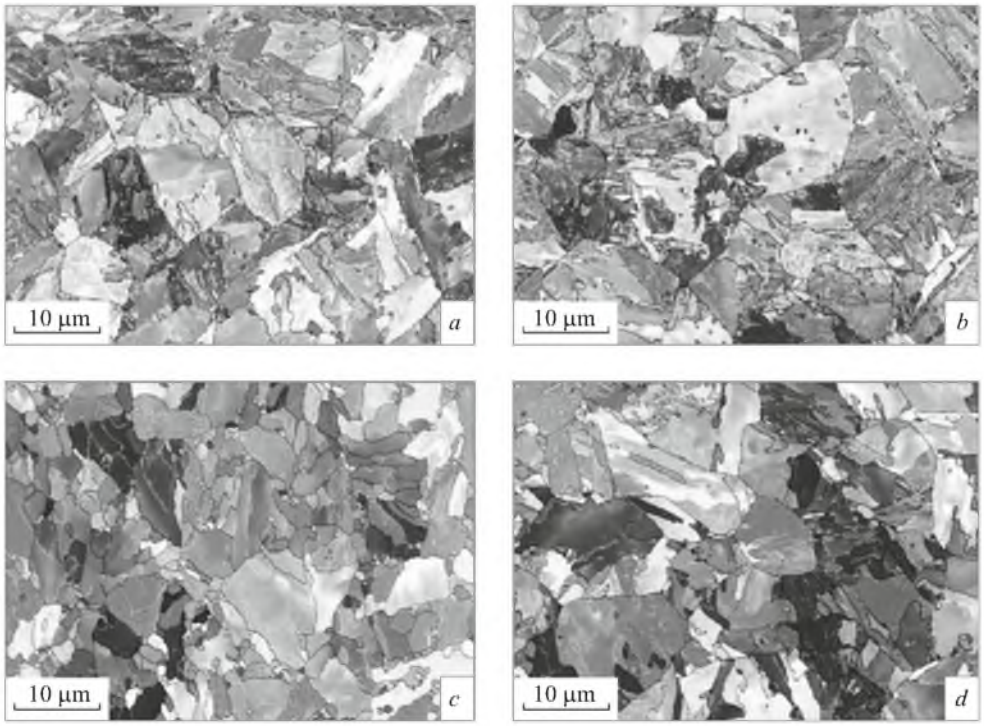

Fig. 3. Maps of off-orientations in steel 10Kh9K3V1M1FBR after hardening from 1050°C (*a*) and tempering for 3 h at 525°C (*b*), 625°C (*c*), and 750°C (*d*).

this assumption (Fig. 4*d*). The size of the RCS was about 40 nm.

Tempering at 300°C did not cause a substantial change in the phase composition of the steel. Only a small amount of Me_3C-type carbides bearing about 85% Fe was segregated additionally; the rest were chromium atoms (Fig. 2*b*).

When the tempering temperature is increased to 525°C, a high amount of carbides is segregated in the martensite (Fig. 5). Films of $Me_{23}C_6$ carbides form over some boundaries of IAG and martensite packets, blocks, and laths (Fig. 6*a*). The fraction of Cr in these films is 70 – 100%; they also contain molybdenum in an amount of 5 – 7%. Unfortunately, we have not managed to obtain data on the crystal geometry of the martensite lath boundaries on which the films were segregated. It should be noted that the formation of film $Me_{23}C_6$ carbides is not connected with the decomposition of austenite; the films nucleate heterogeneously over boundaries. As a rule, formation of film segregations of carbides over LAB causes irreversible temper brittleness in steels and lowers the impact toughness in refractory alloys.

At 525°C we detected additional segregation of nanosize carbonitrides of type Me(C, N) inside martensite laths (Fig. 5*a*). We observed cutting of a carbonitride particle into two by a boundary of a martensite lath, which means that the Me(C, N) particle had existed prior to the beginning of the martensitic transformation (Fig. 5*b*). The picture of segregations due to tempering at 525°C is very complex. Three facts can be mentioned as obviously established ones.

(1) Segregation of round-shape Me(C, N) carbonitrides enriched with niobium (Fig. 5*a* and *d*). The mean size of the round particles decreases to 19 nm and their volume fraction increases. This is a undeniable evidence of additional segregation of carbonitrides.

(2) Segregation of a small amount of $Me_{23}C_6$-type carbides of a plate shape with a mean length of 63 nm and a thickness of 14 nm (Fig. 5*c*). They are positioned primarily over boundaries of IAG and packets, blocks, and laths of

TABLE 2. Parameters of Microstructure of Steel 10Kh9K3V1M1FBR

Heat treatment mode	d_l, nm	ρ, m^{-2}	$d_{s.ph}$, nm	Σ3, %	SAB, %
Hardening from 1050°C	209	$11.7 \cdot 10^{14}$	31	6	73
Tempering at 525°C	205	$9.8 \cdot 10^{14}$	29	7	74
Tempering at 625°C	305	$9.7 \cdot 10^{14}$	43	9	35
Tempering at 750°C	368	$6.2 \cdot 10^{14}$	82	15	44

Notations: d_l) transverse size of martensite laths; ρ) density of lattice dislocations; $d_{s.ph}$) mean diameter of secondary phases; Σ3) fraction of special boundaries in which the number of metal lattice sites per one coinciding site in the common superlattice is equal to 3; SAB) fraction of small-angle boundaries.

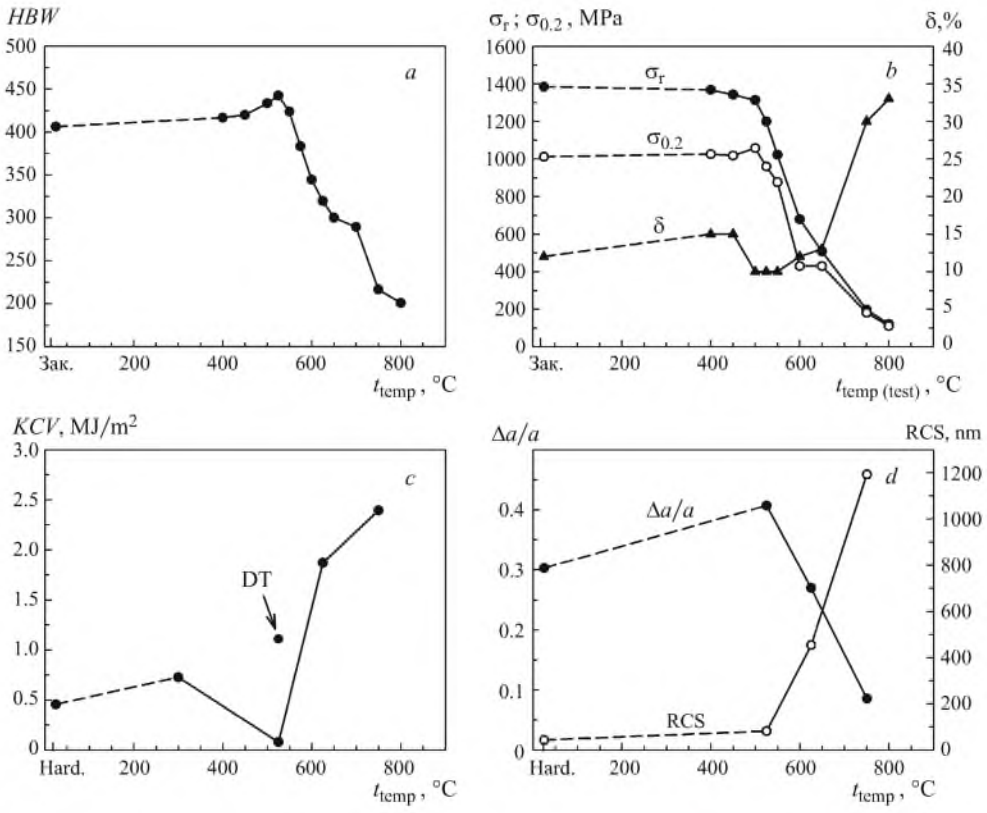

Fig. 4. Dependence of the hardness *HRW* (*a*), impact toughness *KCV* (*c*), microdeformation $\Delta a/a$, and sizes of RCS (*d*) on the tempering temperature and dependence of mechanical characteristics ($\sigma_{0.2}$, σ_r, δ) on the tempering and test temperatures (*b*): Hard) hardening from 1050°C; DT) double tempering at 625°C + 525°C.

martensite, though they may be encountered sometimes in the volume of martensite laths (Fig. 5*c*). In most carbides of type $Me_{23}C_6$ the fraction of Cr is 40 – 50%, the remainder is Fe. Consequently, the chemical composition of the $Me_{23}C_6$ carbides segregated over boundaries in the form of films and in the bodies of martensite crystals differs. Most probably the high content of iron (up to 60%) in these carbides is a sign of their nucleation on cementite particles. This assumption is proved indirectly by the nonuniform distribution of contrast over a $Me_{23}C_6$ carbide in the dark-background photograph given in Fig. 5*c*.

(3) Presence of a great number of round particles of type Me(C, N) with unusually high chromium content. The mean fraction of niobium in them is 63%, that of molybdenum is 1 – 5%, that of vanadium is 7 – 12%, and the remainder is chromium. It should be noted that the proportion of vanadium in the Me(C, N) carbonitrides after tempering at 525°C remains virtually unchanged as compared to the carbonitrides obtained after hardening. It is very unusual that the fraction of chromium in individual carbonitrides attains 56% though the existence of Me(C, N) carbonitrides with such a high content of chromium is impossible in principle [26]. Analysis of the diffraction patterns obtained shows unambiguously that these carbonitrides have preserved an fcc lattice (Fig. 5*d*). The high

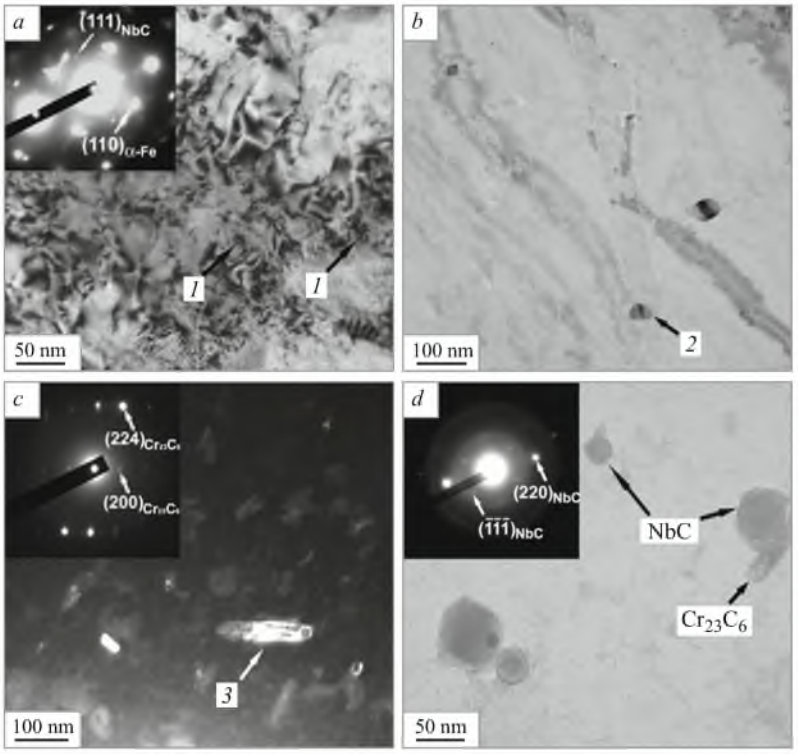

Fig. 5. Microstructure (*a*, *b*) and particles of carbides and carbonitrides on a carbon replica (*c*, *d*) of steel 10Kh9K3V1M1FBR after hardening from 1050°C and 3-h tempering at 525°C: arrows *1* point at particles of type Me(C, N) enriched with niobium; arrow *2* points at a particle of Me(C, N) cut into two by a boundary of a martensite crystal; arrow *3* points at a particle of $Me_{23}C_6$ with nonuniform contrast against dark background.

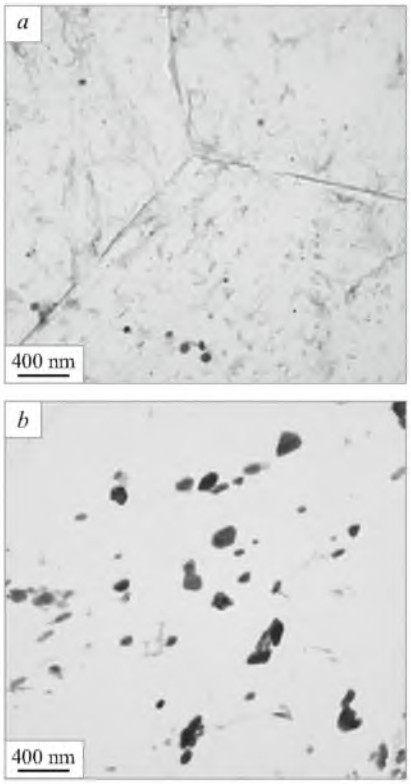

Fig. 6. Carbides in steel 10Kh9K3V1M1FBR on carbon replicas after hardening from 1050°C and 3-h tempering at 525°C (*a*) and 750°C (*b*).

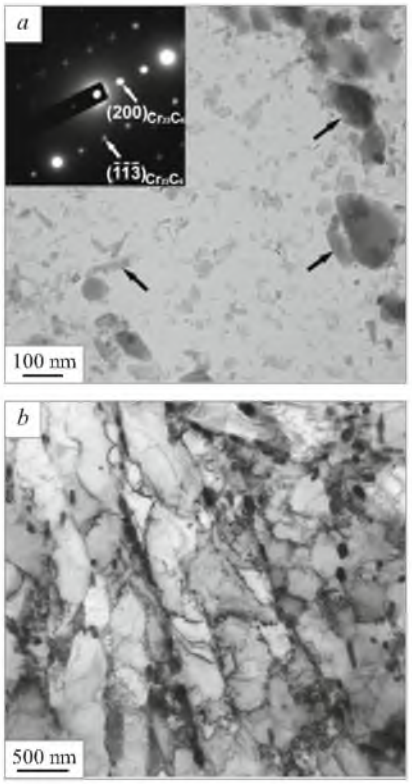

Fig. 7. Particles of $Me_{23}C_6$ carbide in steel 10Kh9K3V1M1FBR on a carbon replica (indicated by the arrows) and diffraction from them after hardening from 1050°C and 3-h tempering at 625°C (*a*) and microstructure of the steel after hardening from 1050°C and tempering at 750°C (*b*).

content of chromium seems to be connected with the fact that carbides of type $Me_{23}C_6$ nucleate on some carbonitrides of type Me(C, N) (Fig. 5*d*).

Most likely, most of the carbides and carbonitrides segregated at 525°C have coherent boundaries, which leads to growth of elastic stresses in the martensite matrix after tempering at 525°C (Fig. 4*d*). Since the dislocation density has decreased inconsiderably (Table 2), the growth in the total level of elastic stresses may be explained only by the contribution of coherent stresses from the phase boundaries along the formed nanoparticles.

We have not observed significant changes in the microstructure after tempering at 525°C (see Fig. 3*b* and Fig. 5*a*). The size of the martensite laths (Table 2) and of the blocks and packets of martensite remains invariable. As a result, the distribution of the off-orientations of the grain boundaries does not change either. Thus, processes of martensite decomposition occur at this temperature; the dislocation structure of the martensite remains virtually invariable.

Tempering at 625°C changes the structure of the steel substantially (see Fig. 3*c* and Fig. 7*a*). A large amount of carbides of type $Me_{23}C_6$ appears in the bodies of martensite laths and over boundaries of IAG, packets, and blocks (Fig. 7*a*). They have the shape of a plate or of a boomerang. Most of these carbides are surrounded by a border of still undetermined nature. It is possible that a region of martensite containing 35% Cr has appeared around these carbides on the carbon replica [27]. The size of carbides of type $Me_{23}C_6$ with lamellar shape after tempering at 625°C is somewhat less than after tempering at 525°C (the mean length is 56 nm and the mean thickness is 14 nm). However, their volume fraction is several times higher and, what is the most important, their composition does not differ from that of the $Me_{23}C_6$ carbides segregated at this tempering temperature over boundaries of IAG and martensite laths; the mean fraction of chromium in them is 66%, that of molybdenum is 2 – 5%, the remainder is iron. In addition, we managed to decipher the diffraction patterns from clusters of these carbides in one reflecting position (Fig. 7*a*), which confirms their appearance in accordance with specific orientation relations. This proves that the carbides belong to type $Me_{23}C_6$. It seems that most of the $Me_{23}C_6$-type carbides have either coherent or semicoherent phase boundaries. After tempering at 625°C we observed niobium-enriched round particles of type Me(C, N) 20 – 80 nm in size. Particles about 25 nm in size with chromium fraction of 80%, molybdenum fraction of 9 – 11%, vanadium fraction of 8 – 12%, and no iron were also encountered. The chemical composition of these phases suggests that these are particles of type $Me_2(C, N)$.

The films of $Me_{23}C_6$ carbides over the boundaries of the IAG and packets, blocks, and laths of martensite transform into round particles with a mean size of about 55 nm. On the

whole the mean size of the particles of secondary phases increases (Table 2). Coagulation of chromium carbides over the boundaries and considerable growth in the volume of these carbides inside martensite laths cause growth in the mean size of the particles of secondary phases. We observed a high amount of uniformly distributed particles with a size of ≤ 20 nm in the bulk of the laths but could not determine their nature.

Thus, growth in the tempering temperature to 625°C is accompanied by additional decomposition of martensite, which leads to growth in the volume fraction of secondary carbides. The thickness of the martensite laths increases by almost a factor of 1.5 and the dislocation density remains virtually unchanged, while the elastic stresses decrease by almost 40% (Fig. 4*d*). The causes of growth of the RCS to almost 450 nm or almost by a factor of 9 (Fig. 4*d*) at constant density of lattice dislocations (Table 2) are unclear. Note that the change in the mean thickness of the martensite laths occurs due to migration of Y-shaped ternary junctions [28]. The thickness of the majority of martensite laths remains unchanged. It seems that this is the reason behind the absence of significant changes in the dislocation density, because the migration of the SAB of martensite laths should necessarily be accompanied by a decrease in the density of lattice dislocations as a result of their capture by the migrating SAB. After tempering at 625°C we observed only LAB of martensite packets (Fig. 3*c*). The boundaries of the blocks acquired a regular shape and passed from one packet boundary to another. Thus, in the range of $t_{temp} = 525 - 625$°C the substructure starts to change and these changes lead to a substantial decrease in the mean off-orientation of the boundaries of packets and blocks of martensite at simultaneous growth in the thickness of the martensite laths. Such processes almost halve the fraction of the SAB (Table 2); the fraction of the LAB with off-orientation of 2 – 5° decreases by a factor of 3. This is possible when the content of dislocation boundaries of martensite increases as a result of migration of an Y-shape junction [28].

Growth in the tempering temperature to 750°C stimulates all the $Me_{23}C_6$-type carbides to acquire a round shape (the mean size is 105 nm). They have incoherent boundaries (Fig. 7*b*) and are arranged in chains over the boundaries of IAG, packets, blocks, and martensite laths (Figs. 6*b* and 7*b*). The composition of the $Me_{23}C_6$-type carbides after tempering at 750°C is the same as after tempering at 625°C. The fraction of chromium in them is 66% on average; the mean fraction of molybdenum is 2 – 5%, the remainder iron. Round-shape niobium-enriched carbonitrides of type Me(C, N) lie inside martensite laths and over their boundaries as well as over the boundaries of blocks. Their size remains the same as after tempering at 625°C. At 750°C the round-shape carbonitrides are accompanied by vanadium-enriched Me(C, N) carbonitrides in the form of lamellar particles 15 nm long and 2.5 nm thick. We may say that at this tempering temperature the process of decomposition of

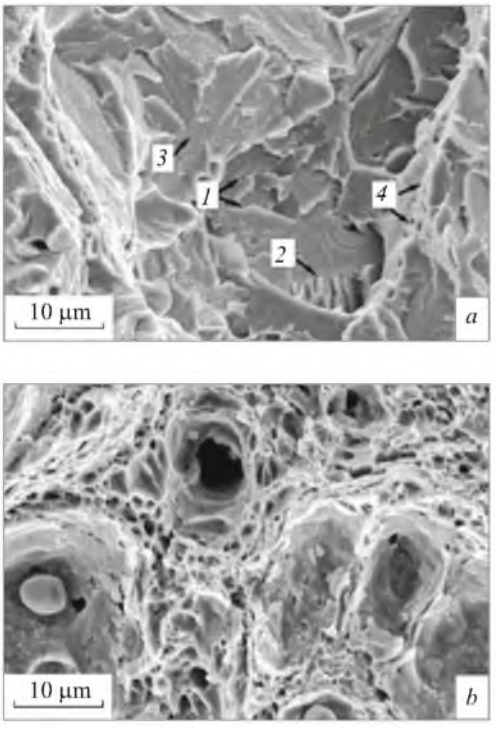

Fig. 8. Fractures formed as a result of impact loading of specimens of steel 10Kh9K3V1M1FBR after hardening from 1050°C and 3-h tempering at 525°C (*a*) and 750°C (*b*): *1* – *3*) facets of quasi-cleavage of different shapes; *4*) region of ductile fracture.

martensite is largely finished. No feature of contrast from coherent stresses was observed around most of the particles of type Me(C, N). The $Me_{23}C_6$-type carbides were frequently surrounded by a border enriched with chromium atoms, which confirms the assumption about their nature made above.

The structure of the steel tempered at 750°C experiences active redistribution of dislocations (Fig. 7*b*), which causes a considerable decrease in the internal elastic stresses (Fig. 4*d*). The decrease in the dislocation density (Table 2) and their redistribution cause a decrease in the size of the RCS. We may say that the dislocations inside large martensite laths are rearranged into well discernible cells, while in the thin martensite laths they enter the longitudinal boundaries and form transverse dislocation boundaries. Consequently, the martensite after tempering has a typical low-energy dislocation structure [29]. Analysis of the maps of off-orientations (see Fig. 3*d*) shows that when the tempering temperature is increased to 750°C, the thickness of the martensite laths increases as well as the sizes of the blocks and packets of martensite. However, the size of the packets and blocks increases by only 5%, while the thickness of the martensite laths grows by 20%. The mobility of the SAB is substantially higher than that of the LAB. These results show that after tempering at 750°C steel 10Kh9K3V1M1FBR acquires the structure of troostomartensite.

Mechanical properties. The effect of the tempering temperature on the hardness is presented in Fig. 4*a*. It can be seen that growth in the tempering temperature is accompanied by increase in the hardness, which acquires a maximum value at 525°C. The hardness of the specimens at this temperature is almost 10% higher than after hardening, i.e., steel 10Kh9K3V1M1FBR behaves as a classical precipitation hardening steel and manifests both primary and secondary hardness. Further growth in the temperature causes a continuous decrease in the hardness. After tempering at 750°C it is almost halved as compared to the maximum value at 525°C. The hardness decreases to 216 *HBW*, which is the maximum value at which steel for power engineering possesses satisfactory weldability and can operate [22, 30]. Consequently, tempering at 750°C with 3-h hold ensures an optimum combination of creep resistance and hardness for grade 10Kh9K3V1M1FBR. The hardness of 206 *HBW* (15 *HRC*), which is treated as optimum for steam conduit pipes [22, 30], can be obtained by tempering at about 770°C. Thus, the temperature dependences of the hardness at $t_{temp} \geq 750$°C for steels 10Kh9K3V1M1FBR and P911 are the same. On the whole, we may state that the tempering temperature for steel 10Kh9K3V1M1FBR can be the same as that for steel P911, which is a cobalt-free commercial version of 10Kh9K3V1M1FBR.

The temperature dependence of the impact toughness correlates well with the curves describing the variation of the hardness. A value of the impact toughness sufficient for operation is obtained after hardening without tempering (Fig. 4*c*). At 525°C the impact toughness exhibits a dip connected with irreversible temper brittleness. Tempering at a higher temperature (625°C) removes this dip (Fig. 4*c*). Second tempering at 525°C after tempering at 625°C decreases the impact toughness by about 40%. However, the value of the impact toughness after the double tempering at 626°C + 525°C is still 14 times higher than that after tempering at 525°C (Fig. 4*c*), which is an obvious confirmation of the main contribution of the mechanism of irreversible temper brittleness to the dip of the impact toughness at this temperature. This effect has not been observed earlier. At the same time, the reversible brittleness observed at this temperature has not been studied in the present work and its mechanism, which differs from that of the irreversible temper brittleness, also contributes to the brittleness at 525°C. The relative value of the impact toughness dip (the difference in the *KCV* after tempering at 625°C and double tempering) matches approximately the data of [13] for a high-chromium steel of the preceding generation. The absolute values of *KCV* for steel 19Kh9K3V1M1FBR (except for the *KCV* at $t_{temp} = 525$°C) are several times higher than in the steels of the preceding generation [13]. It should be noted that the values of the impact toughness after the double tempering match the tendency of growth in the *KCV* upon increase in the tempering temperature (Fig. 4*c*). Tempering at 750°C ensures an impact toughness exceeding the required value by almost a factor of 6.

The temperature dependences of the yield strength $\sigma_{0.2}$ and of the rupture strength σ_r are presented in Fig. 4*b*. At test temperatures of 400 – 500°C steel 10Kh9K3V1M1FBR exhibits a positive temperature dependence of the conventional yield strength. Growth in the deformation temperature promotes an increase in the yield stresses. This phenomenon is quite rare for metallic materials [31]. At 500°C the yield strength $\sigma_{0.2} = 1060$ MPa, which is a very high value for a steel bearing only 0.1% C. Further increase in the test temperature results in a marked decrease in the strength characteristics (Fig. 4*b*). At any test temperature $t_{test} < 650$°C the ratio $\sigma_r / \sigma_{0.2} > 1.3$ and at $t_{test} \geq 750$°C it approaches 1. Consequently, the growth in the test temperature in a range of 650 – 750°C decreases the strain hardening. The elongation δ increases in the range of 20 – 450°C and then decreases by almost a factor of 1.5 despite the fact that $\sigma_r/\sigma_{0.2} > 1.2$, which should ensure satisfactory homogeneity of plastic yielding. At test temperatures above 650°C the ductility increases by almost a factor of 3 despite the fact that at these temperatures $\sigma_r/\sigma_{0.2} \to 1$. Such relation between the strain hardening factor and the elongation is unusual and may be explained only by an early failure caused by formation of cracks.

Fractography. Figure 8 presents fractograms of specimens after tempering at 525 and 750°C. It can be seen that at 525°C fracture occurs by a brittle mechanism, and at 650°C, by a ductile one. After tempering at 525°C the fracture surface bears well discernible quasi-cleavage facets connected by tear-off ridges and shallow dimples (region *1* in Fig. 8*a*). Some of them contain river line steps that show unambiguously that fracture has developed over an intragrain plane (region *2* in Fig. 8*a*). Other important components of cleavage fracture are tongues. These are very thin metal chips (region *3* in Fig. 8*a*). On the other hand, the fracture surface of the specimen contains regions of ductile fracture that develops by merging of micropores (region *4* in Fig. 8*a*). Nucleation of some micropores occurs over the interface of the matrix and a particle with a size ≤ 100 nm (in a dimple). Chemical analysis has shown that all particles in the dimples are enriched with chromium and are most likely carbides of type $Me_{23}C_6$. Regions of ductile fracture can represent grain boundaries or tear-off ridges.

After tempering at 750°C (Fig. 8*b*) the fracture of the specimen is purely ductile. We observed two types of regions, i.e., those with shallow dimples and with large deep dimples, which have appeared on coarse particles enriched with chromium.

DISCUSSION

The data obtained show that the medium-temperature tempering of steel 10Kh9K3V1M1FBR at 750°C results in

the formation the structure of troostomartensite; stable $Me_{23}C_6$ carbides and carbonitrides of type Me(C, N) stabilize the dislocation structure. These carbides form through a number of complex reactions, which affects not only the parameters of the dislocation structure of the troostomartensite formed directly after standard (750°C) tempering but also the processes of the evolution of this structure in creep.

In tempering, the carbide reactions leading to formation of $Me_{23}C_6$ carbides occur differently on the LAB and in the bulk of the martensite laths. This is connected with the fact that the stable $Me_{23}C_6$ carbide has a composite cubic lattice and its nucleation requires simultaneously acting and relatively high concentration and energy fluctuations. Accordingly, the segregation of carbides over boundaries occurs in the following stages:

$$Me_{23}C_6^{film} \rightarrow Me_{23}C_6^{round}. \quad (4)$$

This reaction is accompanied by an increase in the content of Fe in the $Me_{23}C_6$ carbide. The initial segregation of $Me_{23}C_6$ carbides in the form of films in steels of type P92 explains the negative influence of the growth in the sizes of initial austenite grains on the creep resistance [2]. Decrease in the specific surface of grain boundaries upon growth in the size of he IAG and/or increase in the thickness of martensite laths decreases the number of places of heterogeneous nucleation of carbides of type $Me_{23}C_6$ by reaction (4). The mean size of carbides of type $Me_{23}C_6$ segregated over boundaries increases accordingly, which lowers the creep resistance [2]. Simultaneously, the formation of carbides by reaction (1) gives rise to the phenomenon of irreversible temper brittleness.

In the bulk of the laths carbides of type $Me_{23}C_6$ form by a quite different mechanism. The experimental data obtained do not allow us to prove unambiguously the stages of carbide transformation by reaction (1). In any case, even if reaction (1) does occur, most of the $Me_{23}C_6$ carbides form by a simplified scheme

$$Me_3C \rightarrow Me_{23}C_6 \quad (5)$$

by the mechanism of heterogeneous nucleation of $Me_{23}C_6$ on the Me_3C/martensite phase boundaries or on the boundaries of niobium-enriched Me(C, N) carbonitride/martensite at 525°C. At 625°C the mechanism of independent nucleation of a $Me_{23}C_6$ carbide in the martensite matrix comes into play at 625°C. Accordingly, the exothermal peak on the DSC curve is connected with segregation of the $Me_{23}C_6$ carbide. In principle, such mechanisms of change in the stages ensure a uniform distribution of $Me_{23}C_6$ carbides over the martensite matrix with allowance for the close sizes of the particles lying over the boundaries and in the bulk of martensite laths.

The reactions of formation of Me(C, N) carbonitrides do not differ in principle from those observed earlier in steels of the earlier generations [13], except for the fact that the structure does not bear primary coarse Me(C, N) carbonitrides. Such reactions may be written as follows:

$$\text{Martensite} \xrightarrow{525-625^\circ C} \text{Nb(C, N)}, \quad \text{Martensite} \xrightarrow{750^\circ C} \text{V(C, N)}. \quad (6)$$

Note that a part of the Me(C, N) carbonitrides is segregated in the decomposition of austenite at the temperatures given in expression (6), which explains their cutting by martensite laths (Fig. 5*b*) formed at $t < 390$°C (Table 1). In contrast to the steels of the previous generation [13], the formation of Me(C, N) vanadium-enriched carbonitride due to tempering shifts toward higher temperatures. The mentioned fact [7] of equilibrium phase separation of the Me(C, N) carbonitride into niobium- and vanadium-enriched ones is of a primary importance. This ensures formation of a fraction of two nanosize carbonitrides resistant to tempering and creep in steel 10Kh9K3V1M1FBR. These very carbonitrides are responsible for the stability of the dislocation structure of the troostomartensite not only in tempering but also in creep.

The data obtained in the study of the structure show that the possibility of cell formation in the martensite of high-chromium steels appears already at $t_{temp} > 525$°C. Formation of uniformly distributed particles of $Me_{23}C_6$ carbides and Me(C, N) carbonitrides in the volume of the materials decelerates this process and ensures stability of the dislocation structure of the troostomartensite in aging and creep. The stability of the dislocation structure created by nanoparticles and the precipitation hardening due to the nanoparticles themselves raise the creep resistance characteristics of the materials. Steels with such structure possess high parameters of strength, ductility, and impact toughness.

CONCLUSIONS

1. Tempering of steel 10Kh9K3V1M1FBR at 525°C is accompanied by segregation of films of $Me_{23}C_6$ carbide over boundaries of initial austenite grains and packets, blocks, and laths of martensite, which causes irreversible temper brittleness. Tempering at 625°C causes coagulation of the $Me_{23}C_6$ carbide, and this promotes growth in the impact toughness. After double tempering at 625°C + 525°C the impact toughness is 14 times higher than after tempering at 525°C.

2. The process of segregation of $Me_{23}C_6$-type carbides inside martensite laths in steel 10Kh9K3V1M1FBR proceeds in two stages, namely,

$$\text{Martensite} \rightarrow Me_3C \rightarrow Me_{23}C_6.$$

At tempering temperature of 525°C carbides of type $Me_{23}C_6$ form by the mechanism of heterogeneous nucleation on the Me_3C/martensite interfaces or on the interfaces of niobium-enriched Me(C, N) carbonitride/martensite. At 625°C the mechanism of independent nucleation of a $Me_{23}C_6$ carbide in the martensite matrix comes into play.

3. In the process of tempering of steel 10Kh9K3V1M1FBR in the range of 525 – 625°C niobium-enriched Me(C, N) carbonitrides segregate in the form of round-shape particles with a mean size of 19 nm. In the temperature range of 695 – 750°C vanadium-enriched Me(C, N) carbonitrides are segregated in the form of plates up to 15 nm long.

4. In tempering of steel 10Kh9K3V1M1FBR at 525 – 750°C the thickness of the martensite laths increases from 206 to 368 nm, which results in a decrease in the dislocation density and in the volume fraction of small-angle boundaries by a factor of 2.

This work has been performed with financial support of the Federal Agency for Science and Innovations, Grant No. 02.523.12.3019. The authors are grateful to the Collective Use Center "Diagnostics of Structure and Properties of Nanomaterials" of the Belgorod State University for supplying us with the equipment for structural studies and to I. D. Tarasova and E. P. Dan'shina for performing the thermal and x-ray diffraction analyses, respectively.

REFERENCES

1. R. O. Kaibyshev, V. N. Skorobogatykh, and I. A. Shchenkova, "New steels of martensitic class for the heat power industry. High-temperature properties," *Fiz. Met. Metalloved.*, **109**(2), 200 – 215 (2010).
2. A. Belyakov, R. Kaibyshev, V. Dudko, et al., "Effect of heat treatment on microstructure of a 9% Cr steel," in: *Creep & Fracture in High-Temperature Components, 2nd ECCC Creep Conference*, Destech Publications (2009), pp. 1038 – 1045.
3. F. Abe, M. Taneike, and K. Sawada, "Alloy design of creep resistant 9Cr steel using a dispersion of nano-sized carbonitrides," *Int. J. Press. Vess.*, **84**, 3 – 12 (2007).
4. K. Maruyama, K. Sawada, and J.-I. Koike, "Strengthening mechanisms of creep resistant tempered martensitic steel," *ISIJ Int.*, **41**(6), 641 – 653 (2001).
5. F. Abe, "Alloy design of creep and oxidation resistant 9Cr steels for thick section boiler components operating at 650°C," in: *Proc. 4th Int. Conf. on Advances in Materials Technology for Fossil Power Plants, USA*, (2004), pp. 202 – 216.
6. M. Tanura, Y. Haruguchi, M. Yamashita, et al., "Tempering behavior of 9% Cr – 1% Mo – 0.2% V steel," *ISIJ Int.*, **46**(11), 1693 – 1702 (2006).
7. K. Suzuki, S. Kumai, Y. Toda, et al., "Two-phase separation of primary MX carbonitride during tempering in creep resistant 9Cr1MoVNb steel," *ISIJ Int.*, **43**(7), 1089 – 1094 (2003).
8. T. Fujita, "Advances in 9 – 12% Cr heat resistant steels for power plants," in: *Proc. 3rd Int. Conf. on Advances in Materials Technology for Fossil Power Plants, UK* (2001), pp. 33 – 65.
9. W. B. Jones, C. R. Hills, and D. H. Polonis, "Microstructural evolution of modified 9Cr – 1Mo steel," *Metall. Trans.*, **22A**, 1049 – 1058 (1991).
10. R. C. Thompson and H. K. D. H. Bhadeshia, "Carbide precipitation in 12Cr1MoV power plant steel," *Metall. Trans.*, **23A**, 1171 – 1179 (1992).
11. S. Kobayashi, K. Toshimori, K. Nakai, et al., "Effects of boron addition on tempering processes in an Fe – 9Cr – 0.1C alloy martensite," *ISIJ Int.*, **42**, S72 – S76 (2002).
12. J. M. Vitek and R. L. Klueh, "Precipitation reactions during the heat treatment of ferritic steels," *Metall. Trans.*, **14A**, 1047 – 1055 (1983).
13. N. F. Lashko, L. V. Zaslavskaya, M. N. Kozlova, et al., *Physicochemical Phase Analysis of Steels and Alloys* [in Russian], Metallurgiya, Moscow (1978).
14. A. Bjarbo and M. Hattestrand, "Complex carbide growth, dissolution, and coarsening in a modified 12 pct chromium steel – an experimental and theoretical study," *Metall. Mater. Trans.*, **32A**, 19 – 27 (2001).
15. M. Tamura, M. Nakamura, K. Shinozuka, and H. Esaka, "Tempering and precipitation behavior of 7 pct Cr – 0.1 pct V – 0.06 pct Nb – 0.08 pct N steel," *Metall. Mater. Trans.*, **39A**, 1060 – 1076 (2008).
16. N. V. Dashunin, E. P. Manilova, and A. I. Rybnikov, "Phase and structural transformations in 12% chromium steel EP428 due to long-term operation of moving blades," *Met. Sci. Heat Treat.*, **49**(1 – 2), 17 – 18 (2007).
17. H. D. Kim and I. S. Kim, "Effect of austenitizing temperature on microstructure and mechanical properties of 12% Cr steel," *ISIJ Int.*, **34**, 198 – 204 (1994).
18. K. Sawada, K. Kubo, and F. Abe, "Contribution of coarsening of MX carbonitrides to creep strength degradation in high chromium ferritic steel," *Mater. Sci. Technol.*, **19**, 732 – 738 (2003).
19. K. Hamada, K. Tokuno, Y. Tomita, H. Mabuchi, and K. Okamoto, "Effects of precipitate shape on high temperature strength of modified 9Cr – 1Mo steels," *ISIJ Int.*, **35**(1), 86 – 91 (1995).
20. K. Yamada, M. Igarashi, S. Muneki, and F. Abe, "Creep properties affected by morphology of MX in high-Cr ferritic steels," *ISIJ Int.*, **41**, Sup., P. S116 – S120 (2001).
21. M. Taneike, K. Sawada, and F. Abe, "Effect of carbon concentration on precipitation behavior of $M_{23}C_6$ carbides and MX carbonitrides in martensitic 9Cr steel during heat treatment," *Metall. Mater. Trans.*, **35A**, 1255 – 1262 (2004).
22. K. Haarmann, J. C. Vaillant, B. Vandenberghe, et al., *Vallourec & Mannesmann Tubes*, The T91/P91 Book (2002), p. 62.
23. R. Kaibyshev, K. Shipilova, F. Musin, and Y. Motohashi, "Continuous dynamic recrystallization in an Al – Li – Mg – Sc alloy during equal-channel angular extrusion," *Mater. Sci. Eng.*, **396**, 341 – 351 (2005).
24. S. Muneki, H. Okada, H. Okubo, et al., "Creep characteristics in carbon free new martensitic alloys," *Mater. Sci. Eng. A*, **406**, 43 – 49 (2005).
25. B. Jeyaganesh, S. Raju, S. Murugesan et al, "A study on the effect of thermal ageing on the specific-heat characteristics of 9Cr – 1Mo – 0.1C (mass %) steel," *Int. J. Thermophys.*, **30**, 619 – 634 (2009).
26. H. K. Danielsen, J. Hald, F. B. Grumsen, and M. Somers, "On the crystal structure of Z-phase Cr(V, Nb)N," *Metal. Mater. Trans.*, **37A**, 2633 – 2640 (2006).
27. P. Hofer, M. K. Miller, S. S. Babu, et al., "Atom probe field ion microscopy investigation of boron containing martensitic 9 pct chromium steel," *Metall. Mater. Trans.*, **31A**, 975 – 984 (2000).
28. F. Abe, "Coarsening behavior of lath and its effect on creep rates in tempered martensitic 9Cr – W steels," *Mater. Sci. Eng.*, **A387 – 389**, 565 – 569 (2004).
29. B. Bay, N. Hansen, D. A. Hughes, and D. Kuhlmann-Wilsdorf, "Evolution of f.c.c. deformation structures in polyslip," *Acta Metall. Mater.*, **40**, 205 – 219 (1992).
30. *NRIM Creep Data Sheet No. 48*, National Institute for Materials Science, Tsukuba, Japan (2002).
31. A. Courel and D. Caillard, "Prismatic slip in beryllium, I. The controlling mechanism at the peak temperature," *Philos. Mag. A.*, **59**(4), 783 – 800 (1989).
32. K. Sawada, K. Suzuki, H. Kushima, et al., "Effect of tempering temperature on Z-phase formation and creep strength in 9Cr – 1Mo – V – Nb – N steel," *Mater. Sci. Eng.*, **A480**, 558 – 563 (2008).